Environmental Science and Pollution Research (2020) 27:9582–9588
https://doi.org/10.1007/s11356-020-07631-9

RESEARCH ARTICLE

Crayfish shell biochar modified with magnesium chloride and its effect on lead removal in aqueous solution

Jiaqi Zhang[1] · Xiaolan Hu[1] · Jinpeng Yan[1] · Li Long[1] · Yingwen Xue[1]

Received: 24 April 2019 / Accepted: 2 January 2020 / Published online: 9 January 2020

Abstract

In this study, crayfish shell was pyrolyzed at 600 °C to obtain an unmodified biochar (CS600). $MgCl_2$ was used as a modifier to pretreat crayfish shell to produce a modified biochar (CS600-$MgCl_2$) under the same pyrolysis conditions. The two biochars were characterized for physicochemical properties and evaluated for lead (Pb^{2+}) sorption ability to determine the modification mechanism. Mono-element batch adsorption experiments were conducted to compare the sorption performances of CS600 and CS600-$MgCl_2$ to Pb^{2+} in aqueous solutions. All the experiments were carried out at pH of 7. According to the Freundlich–Langmuir model, CS600-$MgCl_2$ had a higher adsorption capacity (152.3 mg/g) than CS600 (134.3 mg/g). FTIR, SEM, XRD, BET, and ICP analyses were applied to inform the interpretation of the mechanism. CS600 was calcium-rich and mainly removed Pb^{2+} through the ion exchange mechanism by replacing Ca^{2+} in the biochar. The increased Pb^{2+} adsorption capacity of CS600-$MgCl_2$ was mainly due to the enlarged specific surface area and the formation of $Mg_3(OH)_5Cl{\cdot}4H_2O$ on the modified biochar. Findings of this study suggest that both CS600 and CS600-$MgCl_2$ can be used to remove heavy metal ions from wastewater and $MgCl_2$ can improve the sorption performance of biochar.

Keywords Lead removal · Crayfish shell · Biochar · Adsorption · Modification · Ion exchange

Introduction

Lead is widely used in industry productions which discharge thousand tons of waste gases, waste waters, and waste residues which contain lead every year. Lead can cause great damage to organism including carcinogenic and mutagenic effects, especially to human beings (Islam et al. 2014). Methods to remove lead in wastes effectively are urgent to be found. Ways including photocatalytic processes (Majidnia and Idris 2016), ultrafiltration (Li et al. 2005), precipitation (Schulte et al. 1996), reverse osmosis (Dialynas and Diamadopoulos 2009), coagulation–flocculation (Pang et al. 2009), nanofiltration (Otero-Fernandez et al. 2018), ion exchange (Kaygusuz et al. 2017), and adsorption (Liu et al. 2013) are common to remove lead. Among these, adsorption has a good research foundation and application cases (Burakov et al. 2018). Adsorbents including active carbon (Kolodynska et al. 2017), carbon nanotubes (Peng et al. 2005), gels (Xie et al. 2008), chitosan (Ngah and Fatinathan 2010), biosorbents (Anayurt et al. 2009), and biochar (Zama et al. 2017) show good adsorption capacity on lead. Compared with other adsorbents, biochar has the advantage of cheap and easy to produce.

There are many studies on the removal of lead from waste water by biochar so far (Li et al. 2017a). Most of these studies use wood-based biochar (Li et al. 2017b; Tan et al. 2018; Wang et al. 2017). Crayfish shell has been found to be a good raw material for biochar (Zeng et al. 2019). The chitosan (Nadarajah et al. 2006) on crayfish shell and the unique structure of it seem to promote adsorption on heavy metals. By the way, crayfish is a kind of popular food in China, which provides a steady source of producing crayfish biochar. Crayfish biochar with no pretreatment has a high adsorption capacity on lead already (Xiao et al. 2017). Therefore, it is of great significance to improve the adsorption capacity of biochar through pretreatment methods such as modification.

Biochar can be modified by organic or inorganic compounds to enhance the adsorption capacity. Modifier includes hydrogen peroxide (Xue et al. 2012), methanol (Jing et al. 2014), polyethylenimine (Ma et al. 2014), and amino groups (Yang and Jiang 2014). The Langmuir adsorption capacity of lead of Douglas fir biochar and its magnetic biochar produced by magnetite (Fe_3O_4) are 16 mg/g and 11 mg/g respectively

Responsible editor: Philippe Garrigues

✉ Yingwen Xue
ywxue@whu.edu.cn

[1] School of Civil Engineering, Wuhan University, Wuhan, China

Table 1 The content of Ca and Mg in different biochar

	Ca/%	Mg%
CS600	16.08	0.313
CS600-$MgCl_2$	8.759	14.77

(Karunanayake et al. 2018). Langmuir values of coconut fiber–derived biochar pyrolyzed at 300 °C and modified with ammonia and nitric acid increase from 49.5 to 105.5 and 85.2 mg/g, respectively, compared to unmodified one (Wu et al. 2017). Hickory wood treated by $KMnO_4$ presents the adsorption capacity of lead at 153.1 mg/g, and surface MnOx particles and oxygen-containing groups are considered as the main adsorption mechanisms (Wang et al. 2015).

The overarching goal of this work is to improve the adsorption capacity of crayfish shell biochar by chemical modification. $MgCl_2$ was used as modifier. It is hypothesized that $MgCl_2$ modification would dramatically improve the physicochemical properties and sorption ability of crayfish shell biochar. The specific objectives are as follows: (1) use $MgCl_2$ to modify crayfish shell to produce biochar, and employ both ordinary biochar and modified biochar to remove Pb^{2+} form liquid solutions; (2) figure out adsorption mechanism and modification mechanism through experiment data and characterization analysis.

Materials and methods

Materials

All chemicals and reagents used in this study were of analytical grades, and the chemical solutions were prepared by deionized (DI) water. Lead nitrate ($Pb(NO_3)_2$) and magnesium chloride ($MgCl_2{\cdot}6(H_2O)$) were purchased from Sinopharm Chemical Reagent Co., Ltd. Crayfish shell was obtained from a commercial source (Wuhan, China).

Biochar production

The original crayfish shell was air-dried. It was put into a quartz tube reactor and slowly pyrolyzed by using a tube furnace in a high-purity nitrogen gas environment. The slow pyrolysis was performed at the temperature of 600 °C for 2 h and the heating rate was 15 °C/min. The produced biochar was ground by a mortar and sieved to a uniform size fraction from 0.9 to 1.2 mm (Hu et al. 2018a; Long et al. 2017). Samples were washed several times with DI water to remove impurities and oven dried at 80 °C. The produced biochar samples were labeled as CS600 and stored for later experiments.

$MgCl_2$ solution was used for modifying crayfish shell. The concentration of the solution was 1.0 mol/L and the ratio of

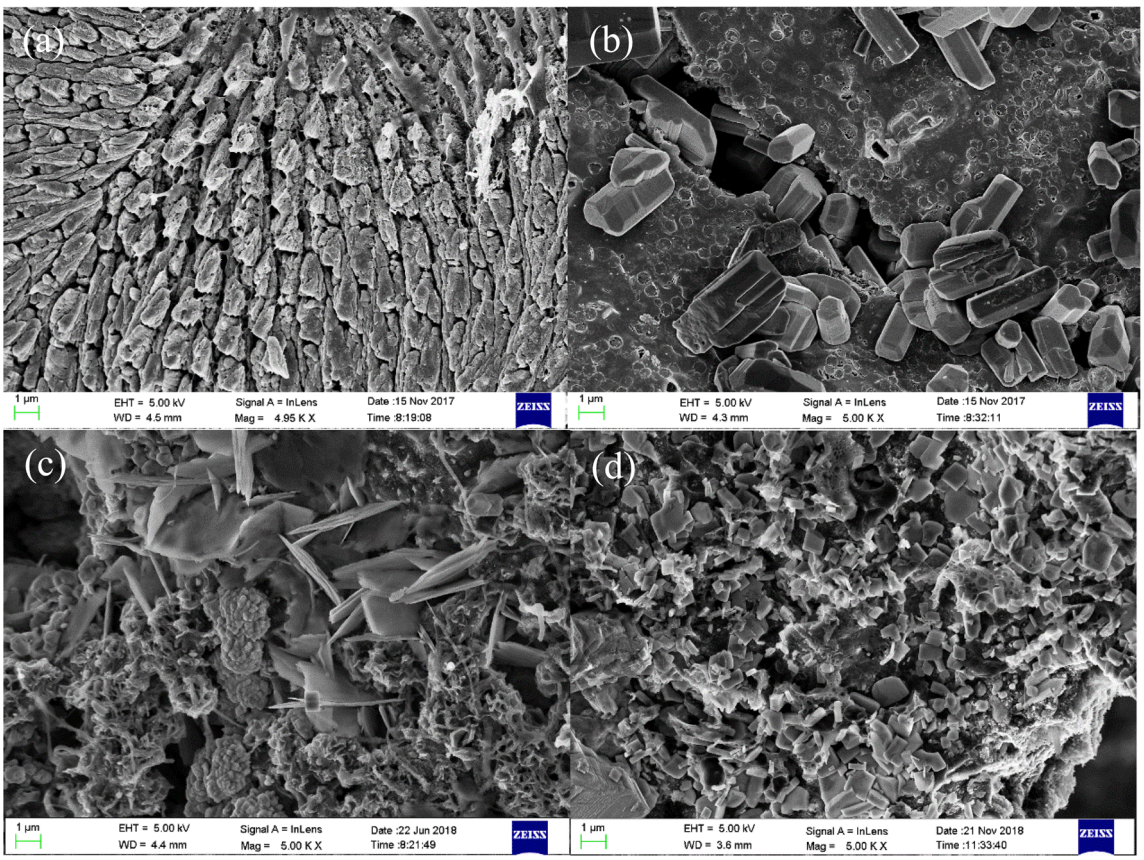

Fig. 1 The scanning electron micrograph (SEM) of **a** CS600, **b** CS600 after adsorption, **c** CS600-$MgCl_2$, **d** CS600-$MgCl_2$ after adsorption

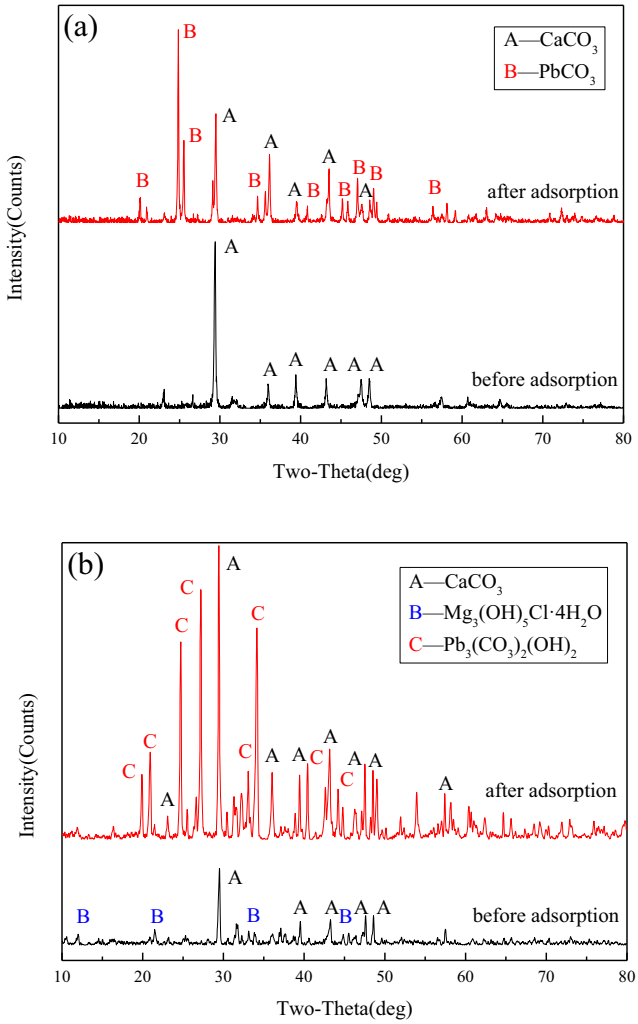

Fig. 2 XRD diffraction patterns of **a** CS600 before and after adsorption, **b** C600-$MgCl_2$ before and after adsorption

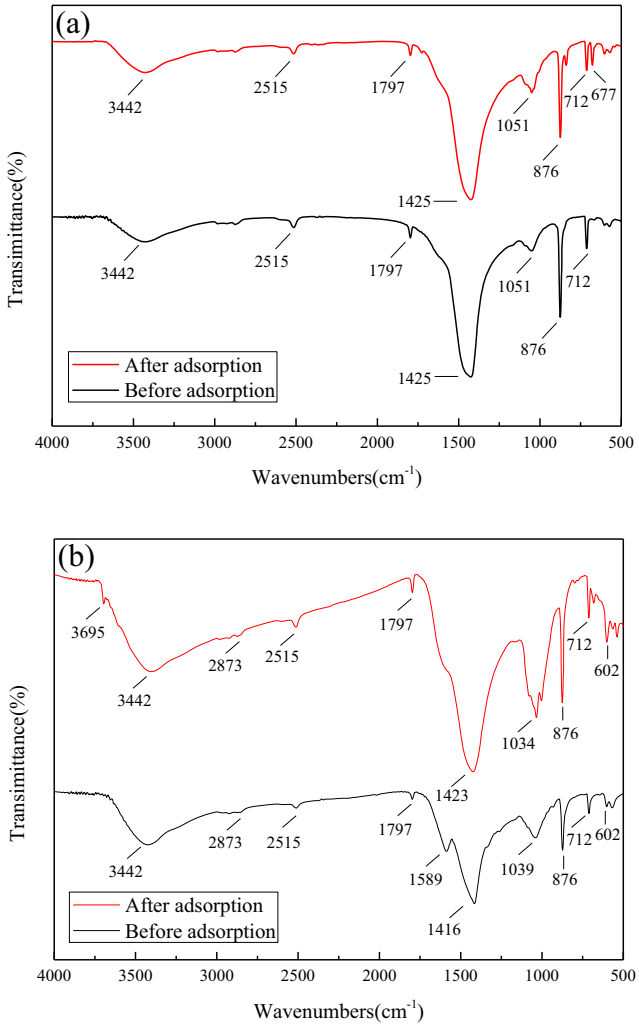

Fig. 3 FTIR spectra of **a** CS600 before and after adsorption, **b** C600-$MgCl_2$ before and after adsorption

crayfish shells to solution was 1 g:2.5 mL. The crayfish shell was soaked in the modification solution for 2 h in the dark and then oven dried, where the temperature was 80 °C. After cooling, the modified feedstock was produced into modified biochar by the same method and labeled as CS600-$MgCl_2$.

Biochar characterization

Biochar was characterized as below. Metal elements (Ca^{2+}, Mg^{2+}, and Pb^{2+}) concentration in modified biochar samples was determined by inductively coupled plasma-atomic emission spectrometry (ICP-OES, Optima 4300DV, Perkin-Elmer SCIEX, USA). Surface area of biochar was measured by TriStar II Automatic surface area analyzer using Brunauer–Emmett–Teller (BET) method. Surface functional groups of biochar were characterized by Fourier-transform infrared spectroscopy (FTIR, Thermo Nicolet, 6700, Madison, WI, USA). Surface morphology of the samples was scanned by field emission scanning electron microscope (Zeiss SIGMA, UK). And crystalline element in biochar was investigated by a computer-controlled X-ray diffractometer (XRD) (PANa-lytical, X'Pert Pro, Netherlands) equipped with a stepping motor and graphite crystal monochromator.

Adsorption kinetics and isotherms

Adsorption kinetics of Pb^{2+} onto biochar were performed by adding 0.1 g different biochar samples into 50 mL of the adsorbate solution in centrifuge tubes at 25 ± 0.5 °C. The concentration of Pb^{2+} in the solution was 500 mg/L, while pH was 7. Adsorbent–adsorbate mixtures were shaken at 120 rpm till sampling at 0.5, 1.0, 2.0, 3.0, 6.0, 12.0, 24.0, and 48.0 h in triplicates. The suspension was immediately filtered through 0.22 μm pore size membrane filters before Pb^{2+} determination. Amounts of Pb^{2+} adsorbed onto biochar were calculated based as the differences between initial and final aqueous concentrations. The adsorption formula can be written as:

Table 2 The assignments of FTIR bands in biochar

Wavenumber (cm^{-1})	Band assignments	References
3442	O–H stretching	Jayawardhana et al. 2019
2515	HCO_3^-	Chang et al. 2019
1797	C=O groups of CO_3^{2-}	
1589	Aromatic stretching	Luo et al. 2015
1425	Calcite out-of-plane bending	Viravaidya et al. 2004
1060–1000	C–O stretching	Kumar and Prasad 2011
876	Calcite in-plane bending	Viravaidya et al. 2004
712	Calcite asymmetric stretching	

$$q_t = \frac{(C_0 - C_t) \times 0.05}{0.1}$$

where q_t is the amount of Pb^{2+} removed at time (mg/g), C_t is the initial concentration of Pb^{2+} in the solutions (mg/L), and C_t is the concentration of Pb^{2+} in the solutions at time (mg/L).

Adsorption dynamics is the relationship between adsorption quantity and time in a continuous period of time after the experiment begins to achieve equilibrium (Zhang et al. 2019a). The transformation of the adsorption quantity and the time of adsorption equilibrium are obtained by the dynamic curve. Pseudo-first-order, pseudo-second-order, and Elovich models were used to describe the adsorption kinetic data. The governing equations of these models can be written as (Hu et al. 2018b):

First-order:

$$q_t = q_e\left(1 - e^{-k_1 t}\right)$$

Second-order:

$$q_t = \frac{k_2 q_e^2 t}{1 + k_2 q_e t}$$

Elovich:

$$q_t = \frac{1}{\beta}\ln(\alpha\beta t + 1)$$

where q_e is the amount of Pb^{2+} removed at equilibrium (mg/g), k_1 and k_2 are the first-order and second-order adsorption rate constants (h^{-1}), respectively, α is the initial adsorption rate (mg/g), and β is the desorption constant (g/mg).

Adsorption isotherms of Pb^{2+} onto the biochar samples were determined according to the same kinetic protocol with different initial Pb^{2+} concentrations (i.e., 10, 25, 50, 100, 200, 300, 400, and 500 mg/L) at contact time of 24 h (Zhang et al. 2019b). The pH of all solutions was 7. The Langmuir, Freundlich, and Langmuir–Freundlich models were used to simulate the adsorption isotherms. The governing equations can be written as:

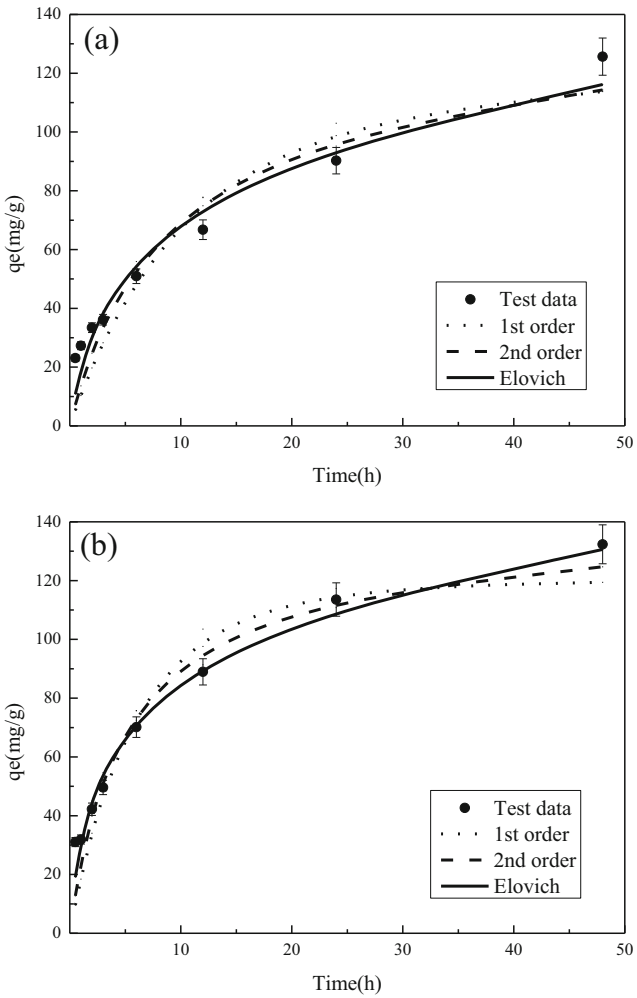

Fig. 4 Adsorption kinetics data and fitted models of heavy metals ions onto **a** CS600, **b** CS600-$MgCl_2$

Table 3 Best-fit parameters for kinetics models of heavy metal adsorption onto modified biochar

Biochar	Model	Parameter 1	Parameter 2	R^2
CS600	First-order	$K_1 = 0.0941$	$q_e = 115.03$ mg/g	0.857
	Second-order	$K_2 = 0.00082$	$q_e = 135.64$ mg/g	0.905
	Elovich	$\alpha = 25.7822$	$\beta = 0.0319$	0.951
CS600-$MgCl_2$	First-order	$K_1 = 0.1677$	$q_e = 119.50$ mg/g	0.890
	Second-order	$K_2 = 0.00149$	$q_e = 137.44$ mg/g	0.943
	Elovich	$\alpha = 545.516$	$\beta = 0.0276$	0.981

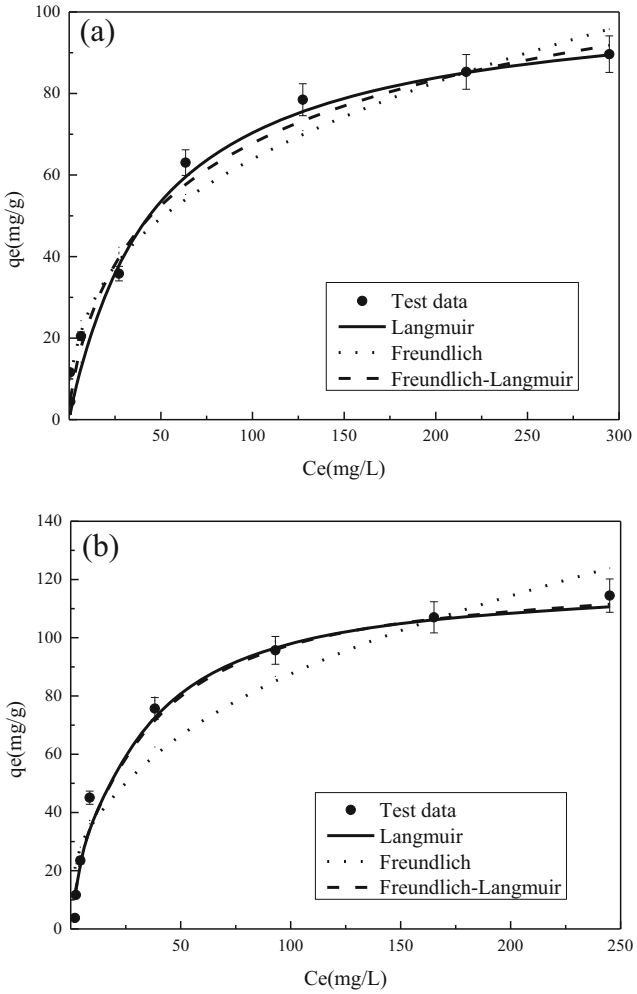

Fig. 5 Adsorption isotherm data and fitted models of heavy metals ions onto **a** CS600, **b** CS600-$MgCl_2$

Langmuir:

$$q_e = \frac{KS_{max}C_e}{1 + KC_e}$$

Freundlich:

$$q_e = K_F C_e^n$$

Langmuir–Freundlich:

$$q_e = \frac{S_{max}(K_{LF}C_e)^n}{1 + (K_{LF}C_e)^n}$$

where K, K_F, and K_{LF} are the Langmuir constant (L/mg), the Freundlich affinity coefficient ((mg/g) $(1/mg)^{1/n}$), and Langmuir–Freundlich constant (L/mg), respectively. S_{max} is the Langmuir maximum capacity (mg/kg), C_e is the equilibrium solution concentration (mg/L) of the adsorbate, and n is the Freundlich linearity constant.

Results and discussion

Physiochemical properties of the produced biochar

Contents of elements (Ca^{2+} and Mg^{2+}) in the produced biochar were obviously affected by modifier magnesium chloride (Table 1). The content of magnesium in CS600-$MgCl_2$ increased significantly, which indicates that modification successfully make magnesium load on biochar. Due to the dehydration and decomposition of $MgCl_2(OH)_6$ at high temperatures (Yin et al. 2019), the surface area of biochar got significantly increased after modification (103.30 m^2/g), which was more than three times larger than the unmodified biochar (31.13 m^2/g).

SEM micrographs showed that the surface of CS600 presented a form with porous structure. After adsorption, a large amount of pseudo hexagonal dipyramidal crystals grew on the surface and inside of biochar. CS600-$MgCl_2$ presented a more abundant porous structure, with flake crystals grew in these pores. And vast bulk crystals in place of flake crystals distributed on the surface of biochar after adsorption (Fig. 1). The result of XRD indicated that crayfish shell biochar was mainly composed of $CaCO_3$. It would be partly replaced by $PbCO_3$ after adsorption. Using magnesium chloride to modify CS600 resulted in the formation of $Mg_3(OH)_5Cl{\cdot}4H_2O$. And $Pb_3(CO_3)_2(OH)_2$ instead of $PbCO_3$ formed after adsorption (Fig. 2).

The FTIR spectrum of the CS600 showed that the characteristic absorption peaks at 1425 cm^{-1}, 876 cm^{-1}, and 712 cm^{-1} were corresponding to out-of-plane bending, in-plane bending, and asymmetric stretching modes of CO_3^{2-} absorption bands of calcite, while peaks at 2515 cm^{-1} and 1797 cm^{-1} can also be attributed to CO_3^{2-}. This undoubtedly confirmed the existence of calcium carbonate in biochar. Other bands in the spectra corresponded to alcoholic O–H (at wavenumber of 3442 cm^{-1}), aromatic ring (1589 cm^{-1}), C–O (1060–1000 cm^{-1}), and C–C. According to Fig. 3a, functional groups of CS600 had little effect on the adsorption of Pb^{2+} onto biochar,

Table 4 Best-fit parameters for isotherm models of heavy metal adsorption onto modified biochar

Adsorbent	Langmuir			Freundlich			Freundlich–Langmuir			
	S_{max}	K	R^2	K_F	n	R^2	S_{FL}	K_{FL}	n_{FL}	R^2
CS600	101.65	0.0250	0.978	12.4495	0.3590	0.972	134.28	0.0111	0.6493	0.985
CS600-$MgCl_2$	119.19	0.0528	0.988	16.3318	0.3684	0.938	152.28	0.0483	0.9455	0.989

because they barely changed before and after adsorption. As Fig. 3b shows, a new peak at 1589 cm^{-1} appeared in CS600-$MgCl_2$, indicating that modification introduced aromatic groups which are beneficial to the adsorption progress. The enhanced O–H (3442 cm^{-1}) can be attributed to the generation of $Mg_3(OH)_5Cl{\cdot}4H_2O$ and $Pb_3(CO_3)_2(OH)_2$ crystals (Table 2).

Adsorption kinetics and isotherms

Adsorption kinetics of Pb^{2+}onto biochar presented two distinct phases: a rapid adsorption phase over the first few hours and another gradually slow adsorption phase until equilibrium (Fig. 4). The adsorption capacity of Pb^{2+} could reach 50% in 6 h, followed by a slower adsorption stage. Pseudo-first-order, pseudo-second-order, and Elovich models are used to simulate the adsorption kinetics data (Table 3). And Elovich model fitted both CS600 ($R^2 = 0.951$) and CS600-$MgCl_2$ ($R^2 = 0.981$) best among them. According to the test data, CS600-$MgCl_2$ recorded the higher amount of Pb^{2+} adsorption equilibrium with 132.3 mg/g, compared with 125.6 mg/g of CS600.

Typical "L" shape presented by adsorption isotherms of Pb^{2+} onto biochar showed that the adsorption capacity increased rapidly at low equilibrium concentrations and had a lag phase when equilibrium concentrations were high (Fig. 5). To better study the adsorption of Pb^{2+} onto biochar, the Langmuir, Freundlich, and Freundlich–Langmuir (F-L) models were applied to fit the data to quantify the change in isotherm shape during the adsorption process (Table 4). The F-L model fitted the data better, and the values of R^2 are 0.985 and 0.989 respectively. In the two kinds of biochar, CS600-$MgCl_2$ showed higher adsorption capacity (152.3 mg/g) than that of CS600 (134.3 mg/g).

Adsorption mechanisms

Since functional groups have little effect on the adsorption of Pb^{2+} onto crayfish shell biochar on the basis of the FTIR spectra, ion exchange plays the major role in adsorption obviously. Pb^{2+}can take place of Ca^{2+} in CS600 and soon form $PbCO_3$. Thus, the adsorption reaction is fast at first. And the difficulty in crystalizing in the pores of biochar might be the reason for the slower adsorption. After being modified by $MgCl_2$, a kind of flake crystal can be scanned in biochar which is $Mg_3(OH)_5Cl{\cdot}4H_2O$. The increase of adsorption capacity of CS600-$MgCl_2$ is mainly caused by the following two reasons. On the one hand, modification helps to improve the specific surface area of biochar a lot, which can promote the ion exchange. On the other hand, ion exchange between Mg^{2+} and Pb^{2+} is prior to that between Ca^{2+} and Pb^{2+}, which can be proved by the formation of $Pb_3(CO_3)_2(OH)_2$.

Overall, the main mechanism for the Pb^{2+} adsorption is metal ion exchange. The replaceable Ca^{2+} and Mg^{2+} are the key to increase the adsorption capacity. CS600-$MgCl_2$ records the higher amount of Pb^{2+} adsorption equilibrium with 132.3 mg/g, compared with 125.6 mg/g of CS600. According to Freundlich–Langmuir model, CS600-$MgCl_2$ shows higher adsorption capacity (152.3 mg/g) than that of CS600 (134.3 mg/g).

Conclusion

In this study, $MgCl_2$ was used as a modifier to improve the adsorption capacity of crayfish shell biochar to lead. The results of XRD, FTIR and metal element concentration analyses indicate that crayfish shell biochar was calcium-rich. The main form of calcium in CS600 was $CaCO_3$, which can exchange Ca^{2+} with Pb^{2+} to form $PbCO_3$ precipitate. This contributes to the high adsorption capacity of CS600 to Pb^{2+}. After modification, lead adsorption capacity of biochar increased from 134.3 to 152.3 mg/g. Several factors contributed to the enhanced lead adsorption on the modified biochar. The modification significantly increased the BET specific surface area of biochar due to the H_2O and HCl gases decomposed from $MgCl_2{\cdot}6(H_2O)$ at high temperature. In addition, the modification also created large amount of $Mg_3(OH)_5Cl{\cdot}4H_2O$ crystals on biochar surface, leading to the ion exchange between Mg^{2+} and Pb^{2+}. Therefore, $MgCl_2{\cdot}6(H_2O)$ modification is an effective method to improve adsorption capacity of crayfish shell biochar to heavy metals. Future research should be carried out to evaluate the desorption and regeneration of CS600-$MgCl_2$.

Funding information This work was partially supported by the National "Twelfth Five-Year" Plan for Science & Technology Pillar Program (grant number 2014BAL04B04), and the Wuhan Water Engineering & Technology Co. Ltd.

References

Anayurt RA, Sari A, Tuzen M (2009) Equilibrium, thermodynamic and kinetic studies on biosorption of Pb(II) and Cd(II) from aqueous solution by macrofungus (Lactarius scrobiculatus) biomass. Chem Eng J 151:255–261

Burakov AE, Galunin EV, Burakova IV, Kucherova AE, Agarwal S, Tkachev AG, Gupta VK (2018) Adsorption of heavy metals on conventional and nanostructured materials for wastewater treatment purposes: a review. Ecotox Environ Safe 148:702–712

Chang HYH, Kuo YL, Liu JC (2019) Fluoride at waste oyster shell surfaces - role of magnesium. Sci Total Environ 652:1331–1338

Dialynas E, Diamadopoulos E (2009) Integration of a membrane bioreactor coupled with reverse osmosis for advanced treatment of municipal wastewater. Desalination 238:302–311

Hu X, Xue Y, Liu L, Zeng Y, Long L (2018a) Preparation and characterization of Na2S-modified biochar for nickel removal. Environ Sci Pollut Res 34:1–9

Hu X, Xue Y, Long L, Zhang K (2018b) Characteristics and batch experiments of acid- and alkali-modified corncob biomass for nitrate removal from aqueous solution. Environ Sci Pollut Res 25:1–9

Islam MS, Ahmed MK, Habibullah-Al-Mamun M, Islam KN, Ibrahim M, Masunaga S (2014) Arsenic and lead in foods: a potential threat to human health in Bangladesh. Food Addit Contam Part A-Chem 31:1982–1992

Jayawardhana Y, Gunatilake SR, Mahatantila K, Ginige MP, Vithanage M (2019) Sorptive removal of toluene and m-xylene by municipal solid waste biochar: simultaneous municipal solid waste management and remediation of volatile organic compounds. J Environ Manag 238:323–330

Jing XR, Wang YY, Liu WJ, Wang YK, Jiang H (2014) Enhanced adsorption performance of tetracycline in aqueous solutions by methanol-modified biochar. Chem Eng J 248:168–174

Karunanayake AG, Todd OA, Crowley M, Ricchetti L, Pittman CU, Anderson R, Mohan D, Mlsna T (2018) Lead and cadmium remediation using magnetized and nonmagnetized biochar from Douglas fir. Chem Eng J 331:480–491

Kaygusuz MK, Isik NO, Erden KE (2017) THE removal of Pb(II) from aqueous solutions by strong and weak acidic cation exchange resins. Fresenius Environ Bull 26:3448–3454

Kolodynska D, Krukowska J, Thomas P (2017) Comparison of sorption and desorption studies of heavy metal ions from biochar and commercial active carbon. Chem Eng J 307:353–363

Kumar JK, Prasad AD (2011) Identification and comparison of biomolecules in medicinal plants of Tephrosia tinctoria and Atylosia albicans by using FTIR. Rom J Biophys 21:63–71

Li CW, Liang YM, Chen YM (2005) Combined ultrafiltration and suspended pellets for lead removal. Sep Purif Technol 45:213–219

Li HB, Dong XL, da Silva EB, de Oliveira LM, Chen YS, Ma LNQ (2017a) Mechanisms of metal sorption by biochars: biochar characteristics and modifications. Chemosphere 178:466–478

Li Q, Gao YT, Lang J, Ding WC, Yong Y (2017b) Removal of Pb(II) and Cu(II) from aqueous solutions by ultraviolet irradiation-modified biochar. Desalin Water Treat 82:179–187

Liu BJ, Lv X, Meng XH, Yu GL, Wang DF (2013) Removal of Pb(II) from aqueous solution using dithiocarbamate modified chitosan beads with Pb(II) as imprinted ions. Chem Eng J 220:412–419

Long L, Xue Y, Zeng Y, Yang K, Lin C (2017) Synthesis, characterization and mechanism analysis of modified crayfish shell biochar possessed ZnO nanoparticles to remove trichloroacetic acid. J Clean Prod 166:1244–1252

Luo L, Xu C, Chen Z, Zhang S (2015) Properties of biomass-derived biochars: combined effects of operating conditions and biomass types. Bioresour Technol 192:83–89

Ma Y, Liu WJ, Zhang N, Li YS, Jiang H, Sheng GP (2014) Polyethylenimine modified biochar adsorbent for hexavalent chromium removal from the aqueous solution. Bioresour Technol 169: 403–408

Majidnia Z, Idris A (2016) Synergistic effect of maghemite and titania nanoparticles in PVA-alginate encapsulated beads for photocatalytic reduction of Pb(II). Chem Eng Commun 203:425–434

Nadarajah K, Prinyawiwatkul W, No HK, Sathivel S, Xu ZM (2006) Sorption behavior of crawfish chitosan films as affected by chitosan extraction processes and solvent types. J Food Sci 71:E33–E39

Ngah WSW, Fatinathan S (2010) Pb(II) biosorption using chitosan and chitosan derivatives beads: equilibrium, ion exchange and mechanism studies. J Environ Sci 22:338–346

Otero-Fernandez A, Otero JA, Maroto-Valiente A, Calvo JI, Palacio L, Pradanos P, Hernandez A (2018) Reduction of Pb(II) in water to safe levels by a small tubular membrane nanofiltration plant. Clean Techn Environ Policy 20:329–343

Pang FM, Teng SP, Teng TT, Omar AKM (2009) Heavy metals removal by hydroxide precipitation and coagulation-flocculation methods from aqueous solutions. Water Qual Res J Canada 44:174–182

Peng XJ, Luan ZK, Di ZC, Zhang ZG, Zhu CL (2005) Carbon nanotubes-iron oxides magnetic composites as adsorbent for removal of Pb(II) and Cu(II) from water. Carbon 43:880–883

Schulte A, Balazs A, Block J, Gehrmann J (1996) Development of heavy-metal deposition by precipitation in West Germany.1. Lead and cadmium. Z Pflanzen Bodenk 159:377–383

Tan GQ, Wu Y, Liu Y, Xiao D (2018) Removal of Pb(II) ions from aqueous solution by manganese oxide coated rice straw biochar - a low-cost and highly effective sorbent. J Taiwan Inst Chem Eng 84: 85–92

Viravaidya C, Li M, Mann S (2004) Microemulsion-based synthesis of stacked calcium carbonate (calcite) superstructures. Chem Commun:2182–2183

Wang HY, Gao B, Wang SS, Fang J, Xue YW, Yang K (2015) Removal of Pb(II), Cu(II), and Cd(II) from aqueous solutions by biochar derived from KMnO4 treated hickory wood. Bioresour Technol 197:356–362

Wang SJ, Guo W, Gao F, Yang R (2017) Characterization and Pb(II) removal potential of corn straw- and municipal sludge-derived biochars. R Soc Open Sci 4:11

Wu WD, Li JH, Lan T, Muller K, Niazi NK, Chen X, Xu S, Zheng LR, Chu YC, Li JW, Yuan GD, Wang HL (2017) Unraveling sorption of lead in aqueous solutions by chemically modified biochar derived from coconut fiber: a microscopic and spectroscopic investigation. Sci Total Environ 576:766–774

Xiao YL, Xue YW, Gao F, Mosa A (2017) Sorption of heavy metal ions onto crayfish shell biochar: effect of pyrolysis temperature, pH and ionic strength. J Taiwan Inst Chem Eng 80:114–121

Xie FZ, Lin XC, Wu XP, Xie ZH (2008) Solid phase extraction of lead (II), copper (II), cadmium (II) and nickel (II) using gallic acid-modified silica gel prior to determination by flame atomic absorption spectrometry. Talanta 74:836–843

Xue Y, Gao B, Yao Y, Inyang M, Zhang M, Zimmerman AR, Ro KS (2012) Hydrogen peroxide modification enhances the ability of biochar (hydrochar) produced from hydrothermal carbonization of peanut hull to remove aqueous heavy metals: batch and column tests. Chem Eng J 200-202:673–680

Yang GX, Jiang H (2014) Amino modification of biochar for enhanced adsorption of copper ions from synthetic wastewater. Water Res 48: 396–405

Yin QQ, Liu MT, Ren HP (2019) Removal of ammonium and phosphate from water by Mg-modified biochar: influence of Mg pretreatment and pyrolysis temperature. BioResources 14:6203–6218

Zama EF, Zhu YG, Reid BJ, Sun GX (2017) The role of biochar properties in influencing the sorption and desorption of Pb(II), Cd(II) and As(III) in aqueous solution. J Clean Prod 148:127–136

Zeng YF, Xue YW, Long L, Yan JP (2019) Novel crayfish shell biochar nanocomposites loaded with Ag-TiO2 nanoparticles exhibit robust antibacterial activity. Water Air Soil Pollut 230:9

Zhang W, Song J, He Q, Wang H, Lyu W, Feng H, Xiong W, Guo W, Wu J, Chen L (2019a) Novel pectin based composite hydrogel derived from grapefruit peel for enhanced Cu(II) removal. J Hazard Mater 384:121445

Zhang W, Wang H, Hu X, Feng H, Xiong W, Guo W, Zhou J, Mosa A, Peng Y (2019b) Multicavity triethylenetetramine-chitosan/alginate composite beads for enhanced Cr(VI) removal. J Clean Prod 231: 733–745